Proc. Lunar Planet. Sci. Conf. 9th (1978), p. 3589–3607.
Printed in the United States of America

A_1 moonquakes: Source distribution and mechanism

YOSIO NAKAMURA

University of Texas, Marine Science Institute, Geophysics Laboratory, Galveston, Texas 77550

Abstract—Two novel analysis techniques have been used to study focal mechanisms of A_1 moonquakes, which occur at the most active of the 80 deep-moonquake source regions identified to date. The first is the cross-spectral analysis of matching signal waveforms. Cross phase spectra clearly show relative polarity of signals and give precise time relationships between signals, thus enabling accurate determination of relative source locations within the source region. The second is the analysis of amplitude ratios, which reveal the patterns of P- and S-wave radiations around the source region. A_1 moonquake foci are found to be concentrated in a nearly horizontal planar region less than 1 km in diameter. Their focal mechanism may be described by slippages along a horizontal plane with the slip direction rotating with and predominantly controlled by the shifting tidal stress field. Thus, A_1 moonquakes represent a process of simple storage and release of tidal energy with no evidence for a release of accumulated tectonic stress.

INTRODUCTION

Moonquakes provide an important clue to the present dynamic state of the lunar interior. Two distinct types of moonquakes have been identified from the lunar seismic data: deep moonquakes (Latham *et al.*, 1971) and shallow moonquakes (Nakamura *et al.*, 1974). Deep moonquakes, which generally occur at depths of 800 to 1000 km, are numerous (more than 100 confirmed yearly) but small; while shallow moonquakes, which are believed to occur at depths less than 100 km, are sparse (average 4 events per year) but preponderantly large.

The most striking feature of deep moonquakes is the clear correlation with the tidal phase of the moon. The monthly periodicity of their occurrence and the seven-month periodicity of their amplitude variation have been clearly demonstrated (Lammlein *et al.*, 1974), and the latest data have also confirmed the expected six-year periodicity of occurrence. Deep moonquakes are small. An estimate by Goins *et al.* (1978) places the total amount of energy released by all the observed deep moonquakes at about 10^{13} ergs per year. This is well within the amount of energy dissipated from the earth-moon system through tides, which is estimated to be about 10^{19} erg/sec (Jeffreys, 1959, p. 240). An important question, then, is whether the tide merely acts as a triggering mechanism for deep moonquakes that releases tectonically accumulated strain energy, or the tide itself is wholly responsible for the existence of deep moonquakes, supplying the required energy inside an otherwise atectonic lunar interior. The answer to this question, therefore, has a great bearing on the matter of the present thermal and dynamic states of the lunar interior.

To answer this question requires detailed knowledge of the source mechanism of deep moonquakes. Unfortunately, however, the complexity of lunar seismic sig-

nals due to intensive scattering and the paucity of seismic stations on the moon preclude application of analysis techniques normally used for earthquake source mechanism studies. Therefore, some new techniques of analyzing the lunar seismic signals are needed.

I have developed two new techniques specifically for this purpose, taking advantage of the complexity of lunar seismic signals: namely (1) cross spectral analysis to obtain polarity of signals and precise relative locations of sources, and (2) amplitude ratio analysis to examine the change of seismic radiation patterns around a moonquake source region. This paper describes the results of applying these techniques to signals from category A_1 deep moonquakes. The results indicate that the tides are not merely the triggering agents, but are the dominant factor in generating deep moonquakes.

A_1 moonquakes

Deep-focus moonquakes are further subdivided into classes, within each of which the signal waveforms are nearly identical throughout the wavetrain for a given station. They are sometimes called matching moonquakes because their waveforms match each other within a class. This is an indication that all moonquakes belonging to a given class are spatially close together defining a source region. We have tentatively identified 80 such classes to date, possibly representing up to 80 source regions.

The most active class identified to date, designated A_1, is comprised of 147 confirmed, separate moonquakes, among which are many of the largest deep moonquakes observed. The class, as defined by a common focal region of very small extent, now includes not only nearly all of the previously identified A_1s but also those tentatively classified as A_{45}, A_{46}, A_{47} and A_{48} by Lammlein (1977).

Table 1 lists the locations of the source region estimated by Lammlein (1977) and Goins *et al.* (1977). The listed locations were determined from P- and S-wave arrival times at the four seismic stations. The source region is southwest of the seismic array. The large spread of the estimates is due mainly to uncertainties in determining the onsets of P and S arrivals on the lunar seismograms. The actual extent of the source region is less than 1 km, or 0.03 degrees, as will be shown later.

In common with all the other classes of deep moonquakes, the occurrence of A_1 moonquakes is strongly correlated with tides raised on the moon by the earth and the sun. One representation of the correlation is shown in Fig. 1, where the location of the sub-earth point (the intersection of the straight line connecting the centers of the earth and the moon with the lunar surface) at the time of occurrence of each A_1 moonquake is indicated by a black dot. The background figures show how the sub-earth point moves on the lunar surface each month as a result of the latitudinal and longitudinal librations of the moon. The third quantity that contributes to the tides on the moon, i.e., the variation in the distance between the earth and the moon, is not explicitly shown in this figure, but it is synchronized with the longitudinal libration. The perigee always occurs when the sub-earth point moves

Table 1. Focal coordinates of A_1 moonquakes estimated by other investigators

Subcategory	Latitude (deg.)	Longitude (deg.)	Depth (km)	Reference
A_1	−10.8	−31.3	900	1
A_1	−13.2 ± 1.9	−31.1 ± 2.6	846 ± 25	2
A_{45}	−16.0	−36.2	964	1
A_{45}	−15.7 ± 2.6	−34.4 ± 3.6	971 ± 28	2
A_{46}	−13.6	−32.5	918	1
A_{46}	−12.5 ± 2.1	−30.4 ± 2.7	879 ± 26	2
A_{47}	−15.0	−40.4	961	1
A_{48}	−17.7	−39.6	1020	1
Range	−14.4 ± 4.0	−34.0 ± 6.4	920 ± 100	

Reference 1: Lammlein, 1977
Reference 2: Goins *et al.*, 1977

from west to east, and the apogee always occurs when it moves from east to west.

The tidal correlation is obvious. A_1 moonquakes occur only at certain phases of the libration each month. They may occur at two opposite phases of the libration within a month depending upon the phase relation between the latitudinal and longitudinal librations. It has been noticed that some A_1 signals also show a reversal of polarity at certain stations.

The observed tidal correlation obviously implies that occurrence of A_1 moonquakes is controlled by the tidal stress variation in the lunar interior. Toksöz *et al.* (1977) and Cheng and Toksöz (1978) have recently attempted to correlate occurrence of A_1 moonquakes with some components of the lunar tidal stress field.

Another tidally correlated feature of deep moonquakes, which is not seen in this figure, is that the observed amplitudes of deep moonquakes are generally large when the amplitude of the longitudinal libration is large, and the variation of the earth-moon distance is correspondingly large, for the month. The librational variation results from the perturbation of the lunar orbit by the sun and can be seen in Fig. 1. The amplitude of the latitudinal libration remains nearly constant because it is mainly due to the tilt of the orbital plane and the equator of the moon relative to the ecliptic.

The present analysis is based on 141 A_1 moonquakes detected through 1975. The data cover a full period of the six-year periodicity for station 12, but successively shorter periods for stations installed in later missions, being reduced down to less than four years for station 16, which was installed in April, 1972.

Cross Spectral Analysis

The first new technique applied to the set of A_1 moonquake signals is the cross spectral analysis. The cross phase spectrum of a pair of matching signals clearly shows whether the two signals are directly matched or matched with the polarity of one of them inverted with respect to the other. In addition, the precise time rela-

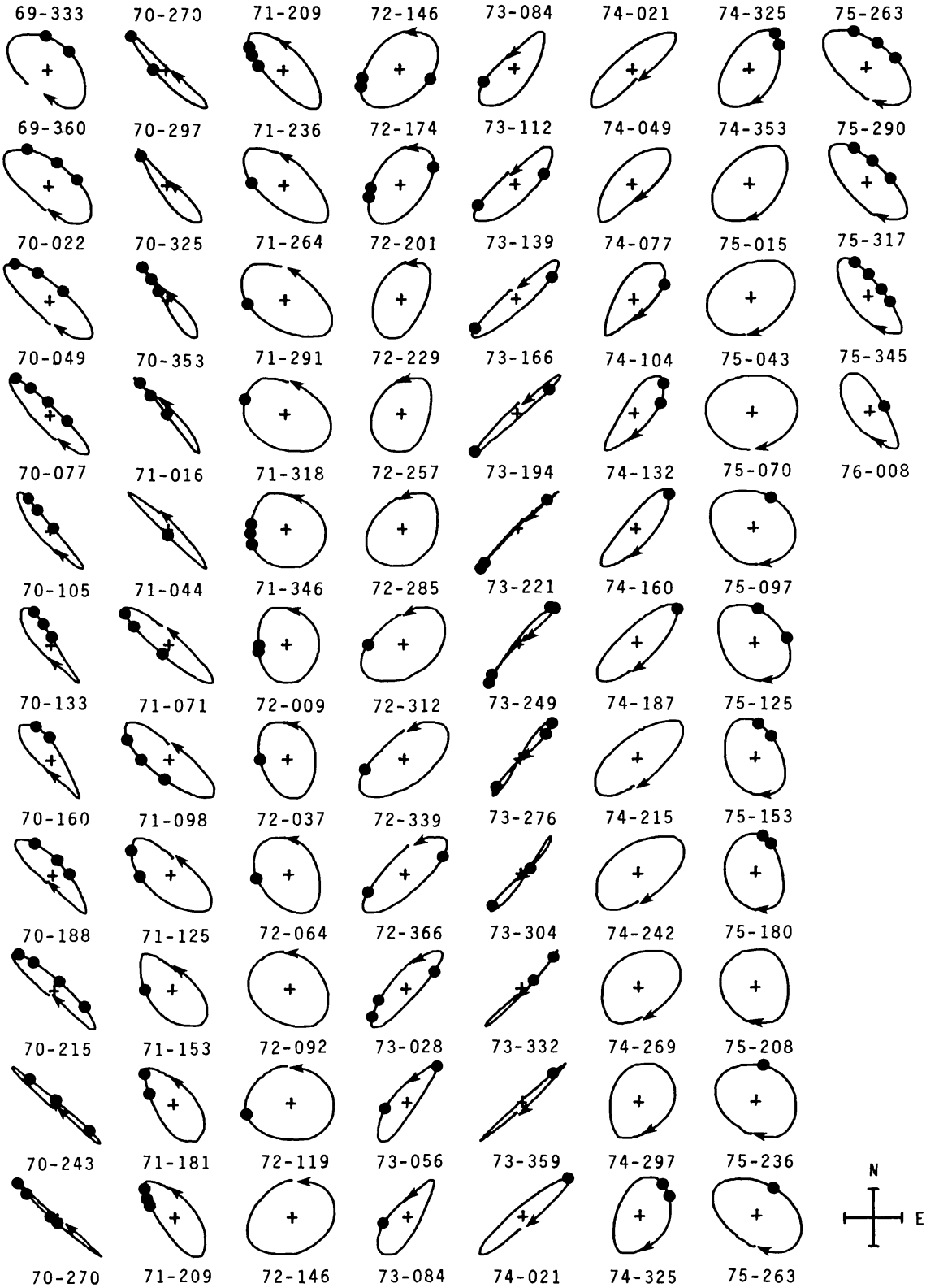

tionship between the signals can be determined from the derivative of the phase with respect to frequency, thus enabling the determination of the relative locations of foci within a source region.

Method and examples

Let two signals, A and B, be given in the form of discrete time series $f_a(t)$ and $f_b(t)$, respectively. Then, the estimates of the coherence spectrum, $C(\omega)$, and the phase spectrum, $\Phi(\omega)$, can be computed by the following formulae (Kanasewich, 1973, p. 115–116):

$$C(\omega) = \frac{(\text{cospectrum of A \& B})^2 + (\text{quadrature spectrum of A \& B})^2}{(\text{power spectrum of A}) \times (\text{power spectrum of B})}, \quad (1)$$

$$\Phi(\omega) = \tan^{-1}\left\{\frac{\text{quadrature spectrum of A \& B}}{\text{cospectrum of A \& B}}\right\}. \quad (2)$$

For deep moonquakes, we are interested in comparing two signals that are nearly identical in waveform except for possible reversal of polarity and observed at different times at a single station. If the two signals A and B were identical in waveform,

$$f_b(t) = k\, f_a(t-\tau), \quad (3)$$

where k is the proportionality constant and τ is the time difference between the signals; then, $C(\omega)$ and $\Phi(\omega)$ would become

$$C(\omega) = 1, \quad (4)$$

and

$$\Phi(\omega) = \omega\tau + \{1 - \text{sgn}(k)\}\pi/2, \quad (5)$$

where sgn(k) is either +1 or −1 depending upon whether k is positive or negative. Equation (5) gives a linear relationship between the phase spectrum and the frequency. It follows that

$$\Phi(0) = \{1 - \text{sgn}(k)\}\pi/2 = 0 \text{ when } k>0 \\ = \pi \text{ when } k<0, \quad (6)$$

and

$$d\Phi(\omega)/d\omega = \tau. \quad (7)$$

Fig. 1. Occurrence times of A_1 moonquakes relative to the libration of the moon. The location of the sub-earth point (the intersection of the straight line joining the centers of the earth and the moon with the lunar surface) at the time of occurrence of each A_1 moonquake is indicated by a black dot. The background figures show how the subearth point moves on the lunar surface each month as a result of the latitudinal and longitudinal librations of the moon. Each figure covers an anomalistic month from an apogee to apogee, with an arrow placed at the end of the month. The numbers between the figures are the year and the day of the year of apogee crossings. The cross at the bottom right corner indicates the scale of ±5 degrees.

Thus, the zero-frequency intercept of the phase spectrum gives the relative polarity of the two signals, and the slope of the phase spectrum gives the time difference between the signals. For real moonquake signals, the waveforms are not perfectly identical. Therefore, the coherence $C(\omega)$ is less than unity. The time difference, τ, however, can still be estimated using relation (7). The accuracy of the estimate, then, depends upon the level of coherence.

Figure 2 shows seismograms of A_1 moonquakes used as standard signals for the analysis. Cross spectra of most of the other A_1 signals up to the end of 1975 have been computed with respect to these standard signals. The sections of the data used for the analysis are indicated by boxes. Each section is about a minute long (400 data samples at 151 msec sampling interval) and starts about 5 seconds before the estimated onset of a P or an S arrival. The raw data are first tapered at both ends using a 64-point (9.7 sec) cosine-bell window, and cross spectral estimates are computed using a Parzen window with a maximum lag of 64 data points. The theoretical accuracy of determination of the time differences from these sets of data, derived from the variance of the cross spectral estimates, is about 5 msec (one standard deviation) when the coherence is 50% over half of the Nyquist frequency. This technique works well for lunar seismograms mainly because the long codas of P- and S-wave arrivals are primarily due to scattering near the stations, and therefore, high coherence of signals is maintained for a long duration of time when a slight relocation of the source takes place. Detailed discussion of this new technique is outside the scope of this paper and will be given elsewhere.

Figure 3 shows two examples of cross phase spectra. Figure 3a compares S-wave arrivals at station 15, and exemplifies signals of identical polarity. Note that the spectrum intercepts the phase axis at 0°. The slight positive slope of the spectrum corresponds to a time differential of about 30 msec, in addition to the time difference indicated at the beginning of the traces. Figure 3b compares S-wave arrivals at station 14, and exemplifies signals of opposite polarity. Note that the spectrum intercepts the phase axis at 180°. The large positive slope of the spectrum corresponds to a time differential of about 450 msec and indicates that the second signal must be delayed by 450 msec, in addition to reversing its polarity to obtain a match with the first signal.

Polarity relations

Polarities of S waves at all stations and P waves at station 14 relative to those of the standard event have been determined for most of the A_1 events recorded by the end of 1975. Those for S arrivals are indicated in Table 2. Blanks indicate either no data, signals too small for analysis, or noisy traces.

Inverted events are found only in 1972, 1973 and 1974, but they are mixed with normal events. Moreover, it is important to notice that the polarity reversal is not always consistently observed at all the stations. There are several instances where the polarity reversal at one station is associated with a signal at another station that is poorly correlated with the standard signal even when the noise level is low. There is even a case where one station shows polarity reversal while another

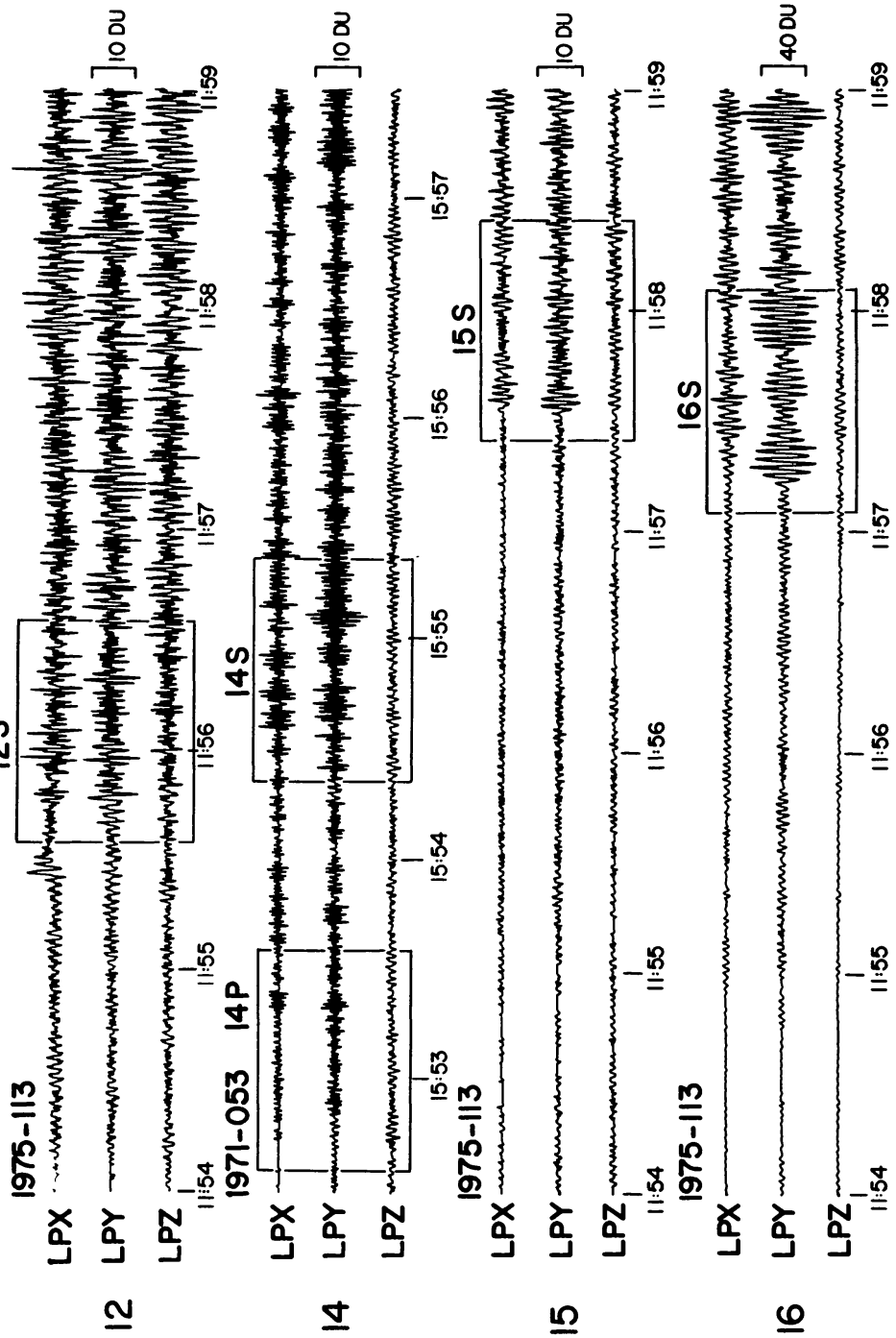

Fig. 2. Seismograms of A_1 moonquakes used as standard signals for the analysis. The numbers at far left are station numbers. LPX, LPY and LPZ stand for two horizontal components and a vertical component, respectively, of long-period instruments. The times are indicated below each seismogram by hours and minutes. DU (digital unit) is the unit of signal digitization performed on the moon, and corresponds to slightly less than 0.1 nm of ground displacement at the peak of the instrument response. Boxes indicate the portions of the signals used for the analysis.

Table 2. List of A_1 moonquakes up to 1975 and observed S-wave polarities

Year	Day	Time[1]	Polarity[2] 12	14	Year	Day	Time	Polarity 12	14	15	16	Year	Day	Time	Polarity 12	14	15	16
1969	344	2131			1971	080	1630	+	+			1973	173	2003				
	347	0720	+			082	2114	+	+				184	0306	−	−		−
1970	006	1328	+			085	0026	+	+				200	0503				
	009	0203	+			107	0612	+	+				201	1901	+			
	010	2305	+			110	0722	+	+				212	0508				
	033	1432	+			137	0536	+	+				226	1939		+		
	035	2040	+			160	1017	+	+				229	1710	+	+		
	038	0132	+			163	0639	+	+				241	0609	−	−	−	−
	061	0152				187	1654	+	+				243	0003	−	−	−	−
	063	0423	+			189	0721		+				253	1057		+		+
	064	2343	+			190	0331		+				270	1745	−	−	−	−
	066	2254	+			216	0715	+	+	+			273	0413	−	−	−	−
	089	1741	+			217	0301		+				281	0907				
	091	0952	+			218	0721	+	+	+			303	0100	−	−	−	−
	093	1048	+			245	2313	+	+	+			321	0730	−	−		−
	116	1430	+			273	2033	+	+	+			330	0234	×	−	−	−
	118	1047	+			299	0006		+				348	0139				
	120	0253	+			327	0519		+			1974	013	1233		−		
	143	1309	+			328	0606		+				099	2149		−	−	
	145	1212	+			329	0919		+				124	2210		−	−	−
	171	0031	+			355	0052		+				127	1946		−	−	−
	173	1157	+			355	1452		+				151	1148	−	−	−	−
	175	0040	+		1972	017	0413	+	+	+			178	2008		−		−
	197	0349	+			044	2125	+	+	+			315	1213		+	×	
	199	0034	+			100	0845						317	0356		+	−	
	201	1143	+			154	0813		+				342	0450		×	−	
	204	0534				155	0619		+		×		343	2346		×	−	−
	226	1826	+			164	2347		−		−	1975	086	1848		+	+	+
	229	0657	+			180	1752		+				113	1154	+	+	+	+
	232	1317				181	1948		+				117	0731		×		
	252	1211	+			195	0505		−		−		140	1728	+	+		+
	254	0814				289	1036		+				142	1554	+	+		
	256	2303				317	2011		−				167	1151	+	+		
	257	1255				345	1759		+				168	2228	+	+		+
	280	0548	+			358	1044		−				221	1303		+		
	284	0937	+		1973	006	0537	×	+				250	0951		+		
	307	1715	+			008	0911		×				276	0623		+		
	334	0236	+			020	0004	−	−		−		278	0747		+		
	336	0407	+			032	1858	+	+				280	0010		+		
	337	1637				050	1255		−		−		304	0635		+		
	361	2034				060	0715	×		−	−		306	0232		+		
	363	1427				088	0639	×		−	−		307	2355		+		
	365	1542				116	1055			×	+		331	0610		+		
1971	028	1459				127	1907	−	−		−		333	0813		+		
	051	1507	+	+		144	1733						335	0116		+		
	053	1553	+	+		156	1111	−	−	−	−		336	0641		+		
	056	1216	+	+		173	1808	+	×				362	1244		+		

[1]Given in hours and minutes of GMT nearest to the first observation.

[2]+ = normal; − = inverted; × = good signal but poor correlation with the standard signal recorded on day 113, 1975.

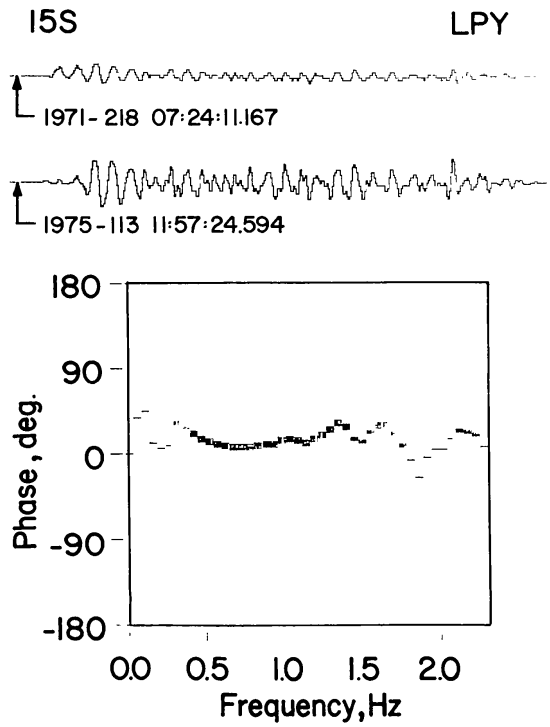

Fig. 3a. An example of a pair of A_1 moonquake signals of equal polarity and their cross phase spectrum. The signals shown are the long-period Y component of S-wave arrivals at station 15. The time of the beginning of each trace is given in year, day of the year, hour, minute and second. The thickness of each short line segment of the spectrum indicates one of the three levels of coherence between signals: a thin line for less than 25% and a thick line for greater than 50% coherence.

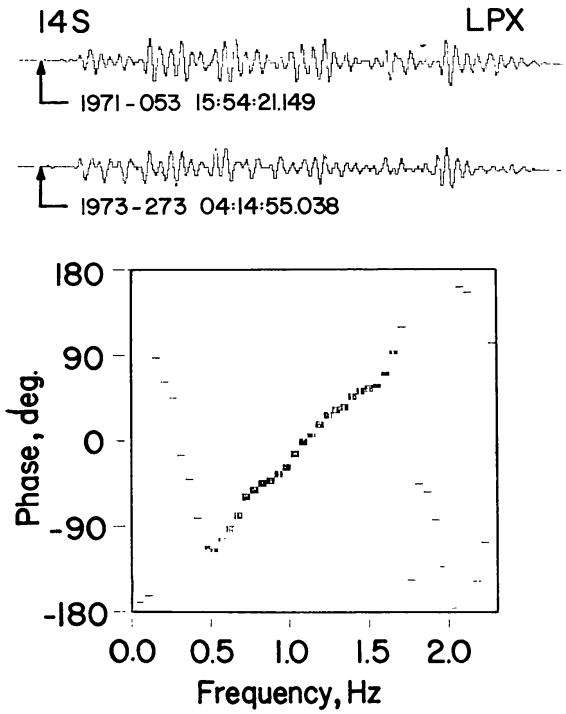

Fig. 3b. An example of a pair of A_1 moonquakes of opposite polarity and their cross phase spectrum. The signals shown are the long-period X component of S-wave arrivals at station 14. See Fig. 3a caption for other explanations.

station shows a normally polarized signal.

If the polarity reversals represent exact reversals of the source orientation, they should be observed consistently at all stations, and the observed waveforms should be exactly opposite of those of normal events. On the other hand, if the source orientation is not exactly reversed, the signal polarity reversal may not be consistent at all stations, and the observed waveforms of S-wave codas will not be exactly opposite of those of normal events. The latter is because S waves are polarized, and the change of the polarization angle other than an exact reversal will change the waveforms of scattered waves which constitute the S-wave coda. (For P waves, the waveforms may still be exactly reversed because P waves, being longitudinal waves, cannot be polarized.) The change of S-coda waveforms are clearly observed (see Fig. 3b for a good example).

Polarity reversal, therefore, does not seem to represent exact reversal of the direction of movement at the source. This point will be further demonstrated in a later section.

Source distribution

The distribution of S-P arrival time differences at station 14 has been determined from the precise measurements of the intervals between P-wave arrivals of pairs of events and those between S-wave arrivals of the same events. The deviations measured are relative to the S-P interval of the standard event on day 113, 1975. The result is shown in Fig. 4. The spread of the S-P intervals is within ±30 msec of that of the standard event. This corresponds to approximately ±240 m in the spread of source distances along the ray direction from station 14 assuming 8 and 4 km/sec for P- and S-wave velocities, respectively, in the source region. Those events whose polarity at station 14 is normal relative to the standard event tend to have shorter S-P intervals (thus closer to station 14) than those whose polarity is inverted relative to the standard event.

In order to determine relative source locations in three-dimensional space, we need relative distances in two additional directions. For this purpose, the distribu-

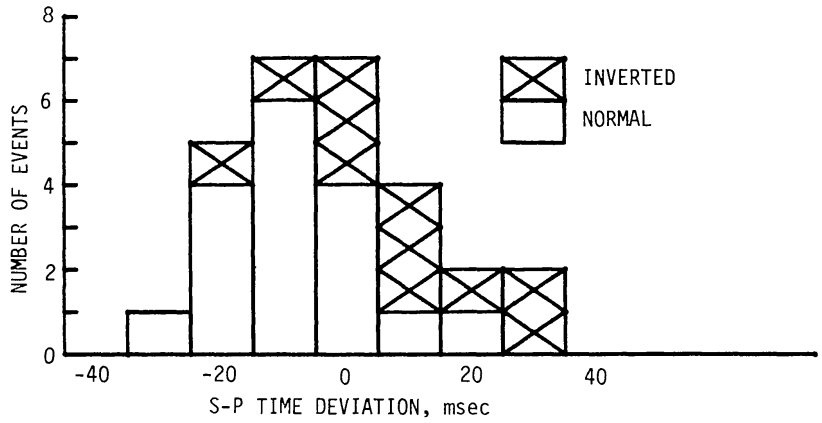

Fig. 4. Distribution of the S-P time intervals of A_1 moonquake signals at station 14 relative to the standard event on 1975 day 113.

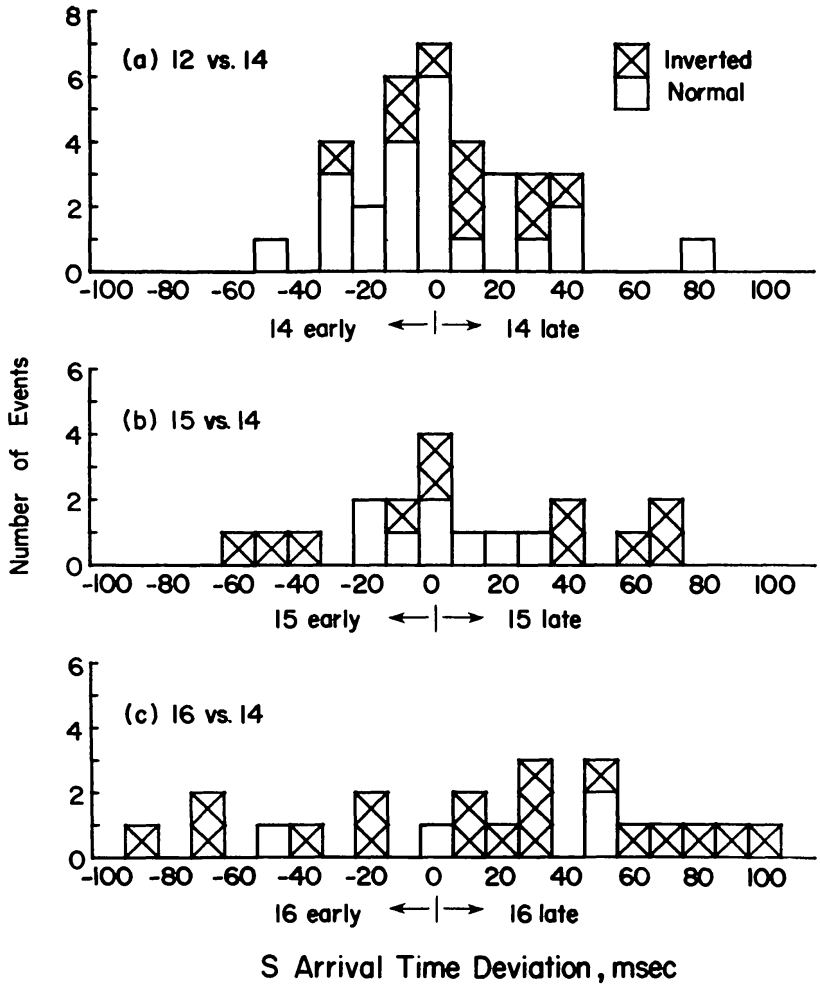

Fig. 5. Distribution of relative S-wave arrival times between stations from A_1 moonquakes. Only deviations from those of the standard event on 1975 day 113 are used.

tions of S arrival time differences between pairs of stations have been determined from the precise measurements of the intervals between S-wave arrivals from pairs of events at all stations. The results are shown in Fig. 5. Inter-station S arrival time differences for the event on day 113, 1975, are again used as the standard, and deviation from these values are computed. The deviations spread farther and more evenly in these distributions, particularly in the last two, than that of Fig. 4.

The actual distribution of moonquake foci in the source region may be obtained by combining the distribution of S-P intervals with those of S-wave arrival time differences. The upper diagram of Fig. 6 shows the source locations projected on the nearly vertical plane through the focus of the standard event and stations 14 and 15. The middle-of-the-range source coordinates of Table 1 are used for the source location of the standard event. The foci are plotted against the time deviations, but the time scale may be considered to be equivalent to a distance scale using appropriate P- and S-wave velocities for the source region. The lower diagram of Fig. 6 shows similar projections on the nearly east-west plane through the focus of the standard event and stations 14 and 16.

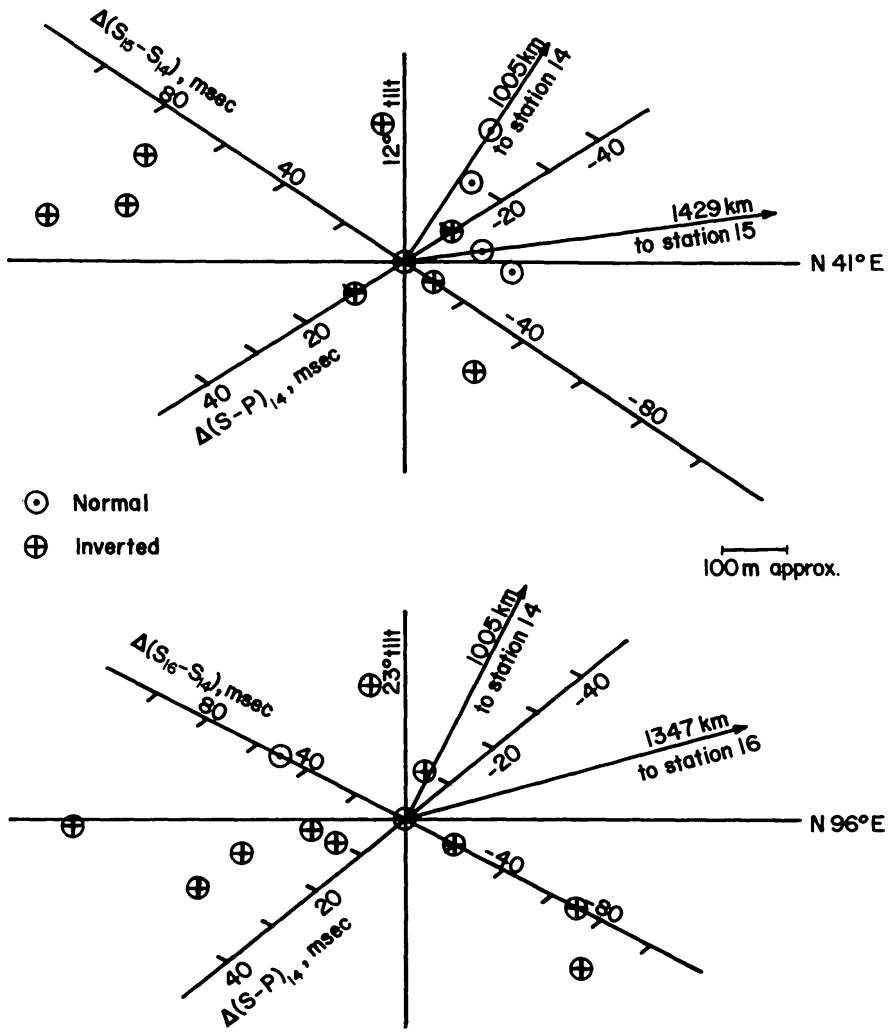

Fig. 6. Relative locations of the A_1 moonquake foci projected on the plane through the focus of the standard event (1975 day 113) and stations 14 and 15 (upper diagram), and on the plane through the focus and stations 14 and 16 (lower diagram). A uniform velocity lunar model is assumed because the observed small variations in seismic velocities do not bend the seismic rays significantly. All lines in each diagram, including the differential time axes, are on the plane. The two planes are slightly tilted from vertical towards southeast and south, respectively, by the angles indicated. The graduated lines are the coordinate axes, against which the data points are plotted. All the other lines are for reference only: the horizontal line, the line perpendicular to the horizontal line, and two vectors pointing towards the two stations. The $\Delta(S_{15\text{ or }16}\text{-}S_{14})$ axis represents $\Delta(S\text{-}P)_{14}=0$, thus is equidistant to station 14 and is perpendicular to the vector pointing towards station 14; while the $\Delta(S\text{-}P)_{14}$ axis represents $\Delta(S_{15\text{ or }16}\text{-}S_{14})=0$, thus is an equi-distance-differential between stations 14 and 15 (or 16) and therefore bisects the angle between the two vectors pointing towards the two stations.

The foci spread out more horizontally than vertically in both projections of Fig. 6. In determining the relative locations of foci, S-wave arrivals at station 14 are used as common data in computing both $\Delta(S\text{-}P)_{14}$ and $\Delta(S_{15\text{ or }16}\text{-}S_{14})$. Therefore, an error in S-wave arrival time at 14 will cause errors of opposite sense in these two quantities. The result will be an elongation of the error ellipse in a nearly

vertical direction in Fig. 6. Thus, the vertical spread of the distribution is more likely to be due to measurement errors than the horizontal spread. With this added consideration, the distribution of foci in the A_1 source region may be described by a nearly horizontal disc of diameter less than 1 km and thickness not more than about 300 m. The orientation of the disc may be somewhat off horizontal. It may be a plane perpendicular to the earth-moon axis as suggested by Toksöz *et al.* (1977).

Amplitude Ratios

Looking at seismograms of A_1 moonquakes in detail, we have noticed for some time that some of them have a clear P arrival while others do not, even when the S arrival is large, and that some events show a large S arrival only at certain stations but not at others. It is further noted that there are systematic changes of the amplitude relations. For example, when multiple events occur consecutively within a month, the first event tends to have the largest P/S amplitude ratio at station 14, while the last event has the smallest ratio. The observed P/S amplitude ratio at station 14 ranges from less than 1/6 to greater than 1/2, with the minimum occurring when the event takes place shortly after a perigee crossing. Such variations of relative amplitude suggest that we are not dealing with seismic sources of constant direction of movement, but rather sources of varying directions.

A model

Considering the earlier observation that the A_1 foci are concentrated around a nearly horizontal plane, and that the P/S amplitude ratio at station 14 appears to be correlated with the anomalistic phase (i.e., the perigee-apogee cycle) of the moon, I have made a tentative, first-approximation model of the A_1 moonquake source mechanism with the following properties. First, it is assumed that there exists a horizontal fault plane along which slippages occur in various directions. Second, it is also assumed that the slip direction rotates at a constant rate, keeping a fixed, linear relation with the anomalistic phase of the moon and completing a rotation every anomalistic month.

Regarding the moonquake focus as a point, P and S amplitudes at large distances may be represented by the radiation pattern of a double-couple point source (Honda, 1957)

$$P \propto V_p^{-3} r^{-1} \alpha \gamma \sin 2\theta \cos \phi, \tag{8}$$

$$S \propto V_s^{-3} r^{-1} \beta \gamma \{(\cos 2\theta \cos \phi)^2 + (\cos \theta \sin \phi)^2\}^{1/2}, \tag{9}$$

where V_p and V_s are the P- and S-wave velocities, r is the distance from the focus to the station, α and β are the P and S attenuation corrections, γ is a station correction, θ is the angle between the normal to the fault plane and the line connecting the focus with the station, and ϕ is the azimuth of the station from the slip direction projected on the fault plane.

The P/S amplitude ratio at a given station and S amplitude ratio between any two stations may be calculated for the model from these equations using appropri-

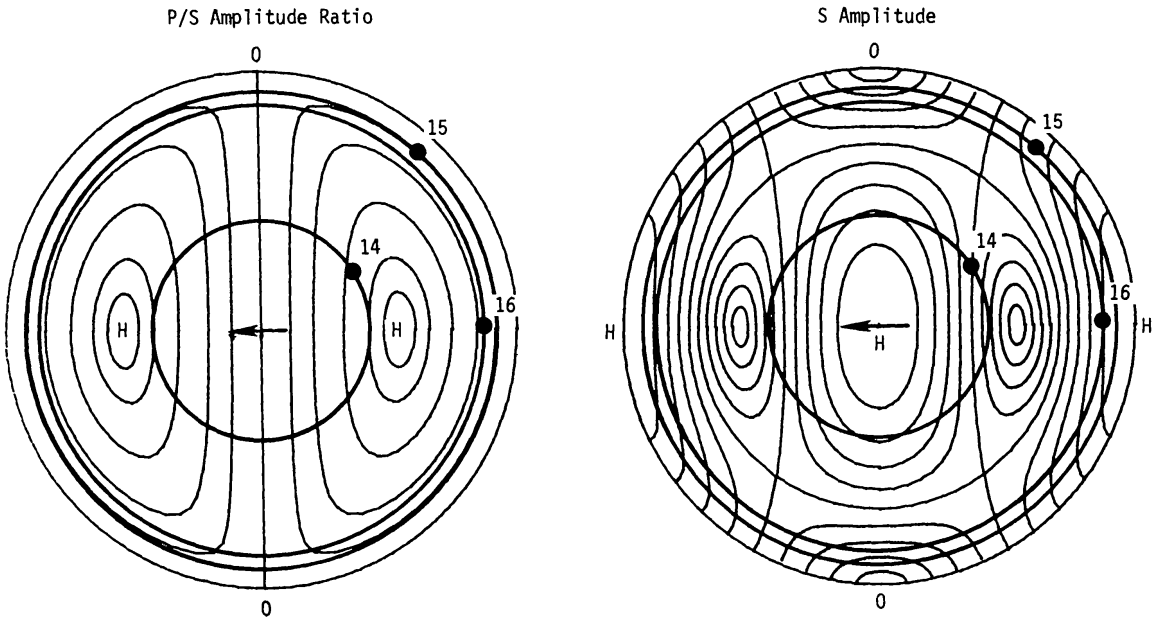

Fig. 7. Theoretical seismic radiation patterns around a double-couple point source projected on a hemisphere above the fault plane. The arrows indicate the direction of the slip vector. The contour lines on the left diagram (P/S amplitide ratio) are at 1/16, 1/8, 1/4, 1/2 and 1 between the nodal line (0-0) and the maxima (H); those on the right diagram (S amplitude) are at every 0.1 of the maximum amplitude. The projections of the stations (black dots) trace the concentric circles as the slip direction rotates.

ate values for the velocities, distances and attenuation and station corrections. The distributions of P/S amplitude ratio and S-wave amplitude, excluding the distance and correction terms, projected on the hemisphere above the fault plane are shown in Fig. 7. The black dots on the figure are the projections of the Apollo seismic stations. Rotating the slip direction is equivalent to moving the stations around the focus on the concentric circles shown in Fig. 7. The variation of amplitude ratios are thus easily discernible from these diagrams. For example, the P/S amplitude ratio shows two minima as the station crosses the P nodal line (0-0) twice when the slip direction makes a complete rotation.

Observations

Envelope amplitudes of P- and S-wave codas measured on standard compressed-scale seismograms are used for amplitude comparisons in this study. I took this approach because the initial arrivals of P and S waves are not always readily identifiable on the seismograms because of the complexity of the signals due to scattering. However, since the P- and S-wave codas are believed to be due to scattering near the station, their amplitudes should be proportional to the amplitudes of the initial P and S waves incident upon the area closely surrounding the station. The amplitudes for the long-period Y component are used for all of the stations.

The P/S amplitude ratios for station 14 are plotted in Fig. 8. The solid lines are the theoretical curves for the model described above. The ratio of S and P attenuations, $\beta/\alpha = 0.68$, is based on the Q's in the lunar interior estimated by Nakamura

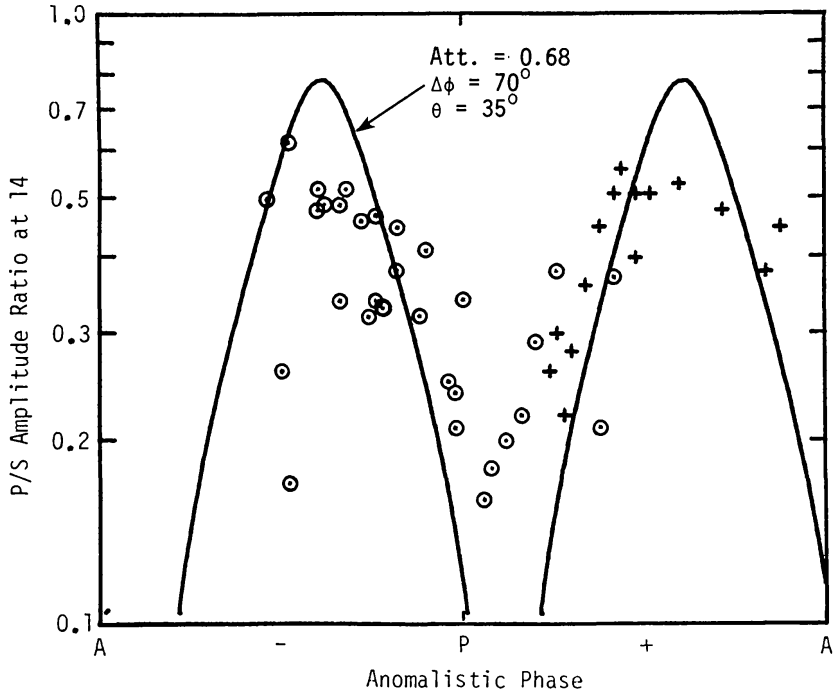

Fig. 8. Observed P/S amplitude ratios at station 14 relative to the anomalistic phase of the moon. Crosses are for clearly inverted events and circles are for all the other events including normal events and those events whose polarities are undetermined. A and P designate apogee and perigee. The theoretical curves are for the model described in the text. $\Delta\phi$ is the azimuth of the slip direction at perigee relative to the projection of the source station line on the fault plane.

et al. (1976). The agreement between the observation and the theory is not perfect, but considering the crude model used, the agreement is quite encouraging. The theory and observation both show a minimum at about 20° (1.5 days) after the perigee crossing. This means that the slip direction at the time is perpendicular to the line connecting the focus and station 14. The somewhat suppressed variation of the observed ratios compared with the theoretical variation may be accounted for by the fact that the envelope amplitude samples incident energy in a wide area around the station.

Figure 9 shows similar plots for the shear-wave amplitude ratios between stations. The theoretical model is exactly the same as the one used for Fig. 8. Again, the agreement between the observation and the theory is not perfect but encouraging.

It should be noted that the apparent good correlation of amplitude variations with the anomalistic phase of the moon does not necessarily mean that the slip direction is controlled only by the anomalistic phase or the earth-moon distance. Deep moonquakes occur only when latitudinal and longitudinal librations are in certain specific relations as seen in Fig. 1. Thus, a correlation with the anomalistic phase also means correlation with the draconic phase, or the latitudinal libration, or any combined effect of tidal variations, and resulting variations of tidal stresses in the focal region.

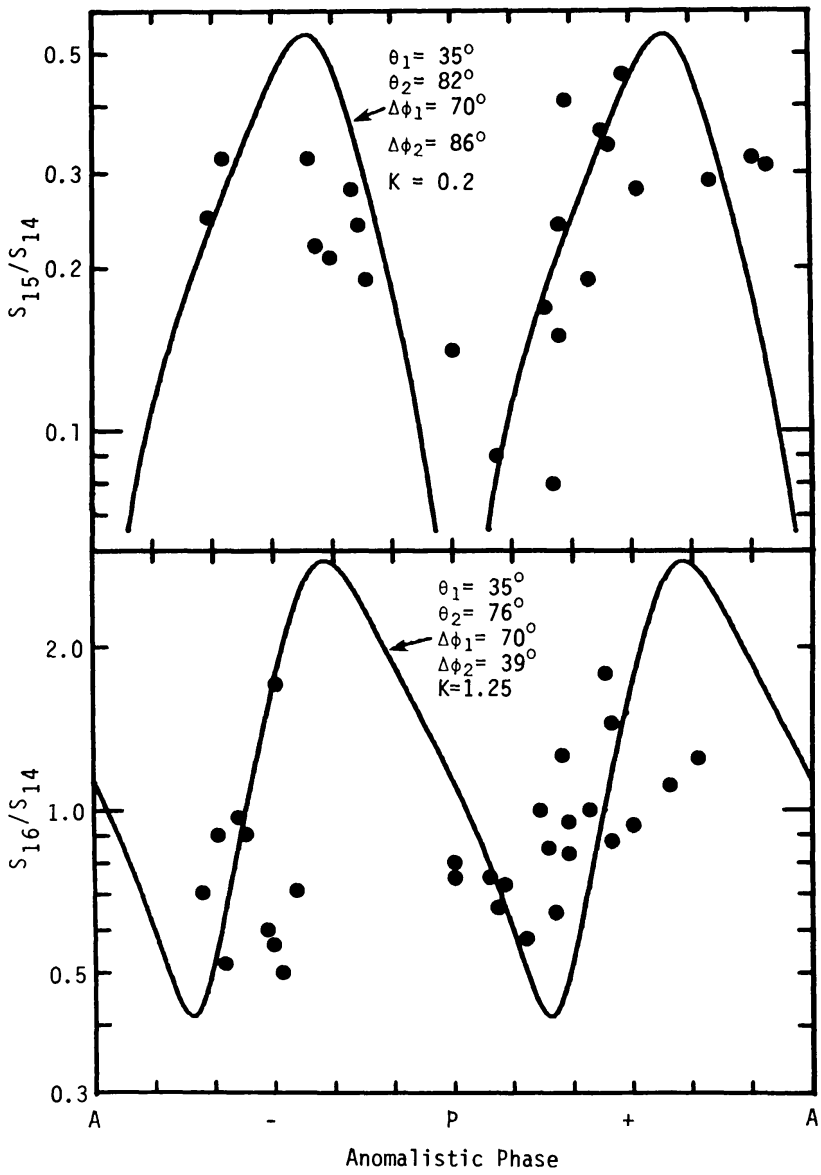

Fig. 9. Observed S amplitude ratios between stations. The theoretical curves are for the model described in the text. K is the net correction factor which is equal to $r_1\beta_2\gamma_2/r_2\beta_1\gamma_1$ of Eqs. (8) and (9), where subscripts 1 and 2 respectively refer to station 14 and one of the other stations.

DISCUSSION

The present analysis using two novel techniques points to the following new findings: (1) A_1 moonquake sources are concentrated on a nearly horizontal plane of less than 1 km in diameter; (2) Observed amplitudes of A_1 moonquakes are consistent with a model in which slippages occur on this plane, not just in any fixed direction and its exact reversal, but in various directions that are controlled by the tides.

The first question one might ask is whether such a small source region is sufficient to generate observed A_1 moonquakes. Goins *et al.* (1978) estimate that the amount of energy released from the largest deep moonquake is of the order of 10^{13} ergs. For this amount of energy to be available from a stress drop of an order of 100 bars (10^8 dyne/cm^2), normally believed to be appropriate for earthquakes, the fault dimension is estimated to be less than 10 m using the formulation of Brune (1970). Even using a stress drop of only 1 bar, which is close to the estimated tidal stress at the depth of deep moonquakes (Cheng and Toksöz, 1978), the fault dimension is of the order of 100 m. In either case, the size of A_1 source region of less than 1 km amply accomodates the expected source sizes of individual moonquakes.

The amplitude ratio analysis definitely indicates that the slip direction at the source is primarily controlled by the tides. If accumulated tectonic strain dominates the deep moonquakes, with the tides acting only as a triggering mechanism, then the slip direction would be nearly constant, contradicting the observation. Thus, we must conclude that the tides cause the deep moonquakes. It is quite probable that deep moonquakes are manifestations of temporary storage and subsequent sudden release of tidal energy at certain selected locations inside the moon where some heterogeneities may produce concentrated tidal stresses sufficient to generate moonquakes. The correlation of the moonquake amplitudes with the amplitude of tidal variations also favors this interpretation.

Ruling out dominant ambient tectonic stress for generating moonquakes in the deep interior of the moon provides a new constraint on the thermal history of the moon. The present thermal stresses due to expansion and contraction of the lunar interior (Solomon and Chaiken, 1976) must be negligible at this depth compared with the tidal stress. The material at this depth certainly is rigid enough to generate moonquakes, and thermal stresses that are not relaxed rapidly enough by plastic flow consistent with this rigidity would have significant control over the mechanism of deep moonquakes.

The present results also lend support to a suggestion by Toksöz *et al.* (1977) and Cheng and Toksöz (1978) that A_1 moonquakes represent slippages on a plane oriented perpendicular to the earth-moon axis, though the orientation may be somewhat different. The dominant role of the tides in generating the deep moonquakes is also confirmed. However, the careful reader might notice that the data and results presented here are not in complete agreement with those of the above authors. First, their analysis was based on only selected A_1 moonquakes (only those moonquakes that occurred near perigee were called A_1's in the preliminary identification). As a result, some of their statements as to the tidal (stress) correlation may not be valid when the complete data set is considered. Secondly, they assumed that A_1 moonquakes are either normal or exactly inverted, and thus required a theory to explain a reversal rather than a rotation of slip motion at the A_1 source. The present study clearly shows that the change of the slip direction is not just a reversal but a rotation on a plane. Thirdly, they concluded that the presence of an ambient or tectonic stress was necessary to explain the observed polarity reversals of the A_1 moonquake signals. This arose partly because they

assumed the exact reversal of the slip direction, and more directly because they did not recognize that long-term tidal stresses are likely to be relieved, leaving only tidal stress variations to be effective in generating moonquakes. No tectonic stress is required by the present study.

Finally, I would like to add that the lunar seismograms are sufficiently different from the terrestrial counterparts in many respects so that some new analysis techniques, such as the ones used in the present study, are often found to be quite beneficial. These techniques may subsequently find some use in analyzing terrestrial seismic signals also. On the other hand, use of some of the techniques well established for the earth may not be suitable under the special conditions found on the moon, and one must exercise caution in applying them to the lunar data.

CONCLUSIONS

A_1 moonquake foci are concentrated on or around a nearly horizontal plane of less than 1 km in diameter. Their focal mechanism may be described by slippages along this fault plane with the slip direction rotating with the shift of the tidal stress field. Thus, A_1 moonquakes represent a process of simple storage and release of tidal energy, not the release of accumulated tectonic energy triggered by tides.

The focal mechanism model used here certainly is a very crude one. More sophisticated models based on computed stress field variations in the focal region will be left for future studies.

Acknowledgments—I wish to thank Drs. Gary V. Latham and H. James Dorman for reviewing the manuscript and offering constructive comments. I also appreciated stimulating discussions with other PSE team members, especially with Dr. Junji Koyama, throughout this study. This research was supported by NASA Contract NAS9-14580 and NASA Grant NSG-7418. University of Texas Marine Science Contribution No. 267. Galveston Geophysics Laboratory.

REFERENCES

Brune J. N. (1970) Tectonic stress and the spectra of seismic shear waves from earthquakes. *J. Geophys. Res.* **75,** 4997–5009.

Cheng C. H. and Toksöz M. N. (1978) Tidal stresses in the moon. *J. Geophys. Res.* **83,** 845–853.

Goins N. R., Dainty A. M., and Toksöz M. N. (1977) The deep seismic structure of the moon. *Proc. Lunar Sci. Conf. 8th*, p. 471–486.

Goins N. R., Toksöz M. N., and Dainty A. M. (1978) Seismic energy release of the moon (abstract). *EOS (Trans. Amer. Geophys. Union)* **59,** 315.

Jeffreys H. (1959) *The Earth*, 4th ed., Cambridge University Press, Cambridge, England, 525 pp.

Honda H. (1957) The mechanism of the earthquakes. *Sci. Rep. Tohoku Univ., 5th ser.*, suppl. **9**, 1–46.

Kanasewich E. R. (1973) *Time Sequence Analysis in Geophysics*, Univ. Alberta Press, Edmonton, Canada, 352 pp.

Lammlein D. R. (1977) Lunar seismicity and tectonics. *Phys. Earth Planet. Inter.* **14,** 224–273.

Lammlein D. R., Latham G. V., Dorman J., Nakamura Y., and Ewing M. (1974) Lunar seismicity, structure, and tectonics. *Rev. Geophys. Space Phys.* **12,** 1–21.

Latham G., Ewing M., Dorman J., Lammlein D., Press F., Toksöz N., Sutton G., Duennebier F., and Nakamura Y. (1971) Moonquakes. *Science* **174,** 687–692.

Nakamura Y., Dorman J., Duennebier F., Ewing M., Lammlein D., and Latham G. (1974) High-frequency lunar teleseismic events. *Proc. Lunar Sci. Conf. 5th*, p. 2883–2890.

Nakamura Y., Duennebier F. K., Latham G. V., and Dorman H. J. (1976) Structure of the lunar mantle. *J. Geophys. Res.* **81,** 4818–4824.

Solomon S. C. and Chaiken J. (1976) Thermal expansion and thermal stress in the moon and terrestrial planets: Clues to early thermal history. *Proc. Lunar Sci. Conf. 7th*, p. 3229–3243.

Toksöz M. N., Goins N. R., and Cheng C. H. (1977) Moonquakes: Mechanisms and relation to tidal stresses. *Science* **196,** 979–981.